



**HAL**  
open science

# Damage Detection in a Wind Turbine Blade Based on Time Series Methods

Simon Hoell, Piotr Omenzetter

► **To cite this version:**

Simon Hoell, Piotr Omenzetter. Damage Detection in a Wind Turbine Blade Based on Time Series Methods. EWSHM - 7th European Workshop on Structural Health Monitoring, IFFSTTAR, Inria, Université de Nantes, Jul 2014, Nantes, France. hal-01020344

**HAL Id: hal-01020344**

**<https://inria.hal.science/hal-01020344>**

Submitted on 8 Jul 2014

**HAL** is a multi-disciplinary open access archive for the deposit and dissemination of scientific research documents, whether they are published or not. The documents may come from teaching and research institutions in France or abroad, or from public or private research centers.

L'archive ouverte pluridisciplinaire **HAL**, est destinée au dépôt et à la diffusion de documents scientifiques de niveau recherche, publiés ou non, émanant des établissements d'enseignement et de recherche français ou étrangers, des laboratoires publics ou privés.

## DAMAGE DETECTION IN A WIND TURBINE BLADE BASED ON TIME SERIES METHODS

Simon Hoell, Piotr Omenzetter

*LRF Centre for Safety and Reliability Engineering, University of Aberdeen, Aberdeen, United Kingdom*

r01sh13@abdn.ac.uk

### ABSTRACT

The interest in renewable energy in the European Union (EU) has increased in the past years, thus efficient energy harvesting becomes more important. For the sector of wind energy, the consequences are growing sizes of wind turbines (WTs) and erections in remote places, such as off-shore. The resulting increase of operation and maintenance costs can be counteracted by structural health monitoring (SHM) systems. Different methods have been developed for detection of damages in WT blades. However, the majority are not suitable for in-service measurements or require dense sensor arrays. This paper presents a damage detection method based on autocorrelations of response accelerations. The damage sensitive feature (DSF) is developed as the Mahalanobis distance between a baseline and a current vector of the autocorrelation coefficients. Firstly, the usefulness of the DSF is assessed by using the Bayes error rate. Secondly, statistical hypothesis testing is utilized for a decision about the structural state. The procedure is applied to numerical simulations of a single WT blade with a disbonding damage scenario. The time series of accelerations are obtained from transient simulations with a simplified aerodynamic loading. The damage detection results show to be sensitive for the chosen damage scenario and are promising for prospective developments of damage detection methods in WTs.

**KEYWORDS:** *Damage detection, Wind turbines, Time series methods, Numerical simulations, Statistical hypothesis testing.*

### 1 INTRODUCTION

Efficient wind energy harvesting becomes more important as a consequence of an increasing interest in, and demand for, renewable energy in the EU [1]. The primary results are growing sizes of WT and erections in more remote places, such as off-shore. This leads to an increase of operation and maintenance costs, which can make up to 20% of the total cost of energy production [2]. SHM can help to counteract this and can lead to increased safety and reliability of WTs.

Structural damage in WT blades caused up to 19.4 % of WT failure incidents in the past [3], where the main reasons were fatigue, extreme gust wind and lightning strikes. Therefore, damage detection in blades deserves high attention. The majority of the existing methods for composite WT blades are suitable only for postproduction testing and verification, e.g. thermal imaging, ultrasonic and laser Doppler vibrometer methods. To benefit from a SHM system, a continuous monitoring of the structural state is required, and currently available methods are acoustic emission and strain monitoring [4]. However, these methods are capable to detect only local damages, thus dense arrays of sensors are necessary to monitor the whole structure. This increases instrumentation and data analysis costs.

The method presented in this paper is based on time series analysis of accelerations. It is known that the responses of structures change when their stiffness is reduced due to damage, and vibration-based damage detection methods use this behaviour. The developments of these methods

can be categorized into three groups. The first group utilizes changes in estimated parametric models of response signals. For example, Nair et al. [5] demonstrated theoretically the relationship between structural stiffness and autoregressive (AR) coefficients, and multivariate AR models have been used for condition monitoring of a 5 MW offshore wind energy converter [6].

The second group uses non-parametric time series representations, which have the advantage of omitting the model structure selection and model parameter estimation steps. A classical approach is the analysis of frequency response functions (FRFs). The calculation of FRFs requires knowing the excitation force. This is generally not possible for large structures like WT blades. Ghoshal et al. [7] presented an integral damage indicator based on the transmittance function (TF) between two sensor positions. The use of the TF has the advantage that the excitation force is cancelled out and does not need to be measured.

Modal-based methods use changes in modal parameters, such as natural frequencies, modal damping ratios and mode shapes, for the damage detection and form the third group. The identification of the underlying dynamic system from output-only data can be done with operational modal analysis techniques [8], e.g. subspace-identification, frequency domain decomposition and eigensystem realization - natural excitation technique.

A unified statistical framework for time series-based SHM has been presented by Fassois et al. [9]. Statistical hypothesis testing is proposed in that paper for decision making about the current structural state. The approach is directly applicable for parametric and non-parametric time-series methods and, under certain assumptions, can be extended to modal-based methods.

The method proposed in this paper uses the autocorrelation function estimates for damage detection. The next section gives a detailed description of the proposed method. Then, numerical simulations of a single WT blade with simplified aerodynamic loading and several disbond damage scenarios are presented. The results of the damage detection are shown in the following section. Finally, a discussion of the results and prospects for future work are given in the last section.

## 2 METHODOLOGY

The aim of the proposed method is the detection of structural damage. Therefore, the estimates of the autocorrelation coefficients at selected sensor locations are used. This methodology allows analysing signals from different locations separately. Unbiased estimates of the autocorrelation function for a discrete time series  $x[k]$  with  $N_{samp}$  samples can be calculated by [10]:

$$\hat{R}_{xx}[\tau] = \frac{1}{N_{samp} - \tau} \sum_{k=1}^{N_{samp}-\tau} x[k]x[k + \tau] \quad \text{for } \tau = 0, 1, 2, \dots, m \quad (1)$$

The proposed DSF is related to the squared Mahalanobis distance between the vectors of the first  $m$  autocorrelation coefficients obtained from different measurements. Firstly, the Bayes error rate is utilized to assess the usefulness of the chosen feature. It is a theoretical value of the misclassification rate between two classes for a certain feature, and it is herein used as an indicator for the detectability of damages with different extents. The upper bound for the Bayes error can be calculated with [11]:

$$E_{Bayes} \leq \frac{2P_b P_d}{1 + P_b P_d D^2} \quad (2)$$

where  $P_b$  and  $P_d$  are the a priori probabilities that an arbitrary pattern belongs the baseline and the damaged data, respectively, with  $P_b \geq 0$ ,  $P_d \geq 0$  and  $P_b + P_d = 1$ . The squared Mahalanobis distance  $D^2$  between the two distributions is given by the mean feature vectors,  $\bar{R}_{bb}$  and  $\bar{R}_{dd}$ , and the pooled covariance matrix  $C_{sp} = P_b C_b + P_d C_d$  as

$$D^2 = (\bar{R}_{bb} - \bar{R}_{dd})^T C_{sp}^{-1} (\bar{R}_{bb} - \bar{R}_{dd}) \quad (3)$$

The matrices  $C_b$  and  $C_d$  are the covariance matrices of the baseline and the damage state, respectively. In the case of the herein used simulation data, the covariance matrices were singular. Therefore, the Moore-Penrose pseudo invers is used instead of the traditional inverse. Here, only

entries corresponding to non-singular eigenvalues are inverted and the remaining entries are set to zero.

In contrast to the classification error estimation above, the detection phase employs a statistical hypothesis testing approach, where only information about the baseline pattern distribution is required. It is assumed that the difference  $\Delta\hat{R}$  between a baseline and a current vector of estimated auto-correlation coefficients,  $\hat{R}_{bb}$  and  $\hat{R}_{cc}$ , respectively, follows a multivariate Gaussian distribution [9]:

$$\Delta\hat{R} = \hat{R}_{cc} - \hat{R}_{bb} \sim \mathcal{N}(R_\delta, C_\delta) \quad (4)$$

with the true mean  $R_\delta$  calculated as the difference of the true autocorrelations of the baseline and the current model,  $R_{bb}$  and  $R_{cc}$ , respectively:

$$R_\delta = R_{cc} - R_{bb} \quad (5)$$

and the true covariance matrix  $C_\delta$  with the covariance of the current state  $C_c$  as

$$C_\delta = C_c + C_b \quad (6)$$

However, if the structure is undamaged then the difference follows a zero-mean Gaussian distribution with covariance  $C_\delta = 2C_b$ . In this case, the squared Mahalanobis distance as a squared sum of independent Gaussian variables follows a central chi-square distribution

$$D^2 = \Delta\hat{R}^T C_\delta^{-1} \Delta\hat{R} \sim \chi_d^2 \quad (7)$$

The true covariance  $C_b$  is generally unavailable, thus the estimated version  $\hat{C}_b$  is used for computation. The number of degrees-of-freedom  $d$  is usually the dimension of the feature vector, but if the pseudo invers is used for calculating the distance, as in our case, then  $d$  corresponds to the number of non-zero eigenvalues.

The hypothesis testing problem can be defined as

$$\begin{aligned} H_0 : \Delta R = R_{cc} - R_{bb} = 0 & \quad (\text{Null Hypothesis, undamaged}) \\ H_1 : \Delta R = R_{cc} - R_{bb} \neq 0 & \quad (\text{Alternative Hypothesis, damaged}) \end{aligned} \quad (8)$$

This enables to define a test of the Mahalanobis distance with a defined level of significance  $\alpha$  for the cumulative chi-square distribution function with  $d$  degrees of freedom  $F_{\chi_d^2}(1-\alpha)$  as

$$\begin{aligned} D^2 < F_{\chi_d^2}(1-\alpha) & \Rightarrow H_0 \text{ is accepted} \quad (\text{undamaged}) \\ \text{Else} & \Rightarrow H_0 \text{ is rejected} \quad (\text{damage occurred}) \end{aligned} \quad (9)$$

### 3 SIMULATION

The proposed methodology for damage detection is applied to a numerical model of a large WT blade. The specifications are taken from the SNL 61.5m reference blade [12], which was designed on the basis of the NREL 5 MW reference WT [13]. The structural design was done according to the international standard IEC 61400-1 Ed. 3 [14] and the baseline properties of the reference WT. With the help of these references and the SNL Matlab Toolbox NuMAD [15], an ANSYS Mechanical [16] FE model of a single blade has been created. Element type and mesh size studies led to a baseline model with 1650 SHELL281 elements.

Disbonding of blades is an important damage type for large WT blades [17]. Jensen et al. [18] performed a full scale structural test on a 34 m long WT blade until failure for flap-wise bending. A disbonding of the outer skin from the load carrying box girder was observed. They assumed that the corresponding reduction of buckling capacity had the main influence on the collapse. According to this observation, disbonding of a single shear-web from the high pressure cap is chosen as damage scenario. The initial location is defined as the maximum chord location, because this area is found to be prone to damages from real inspections [19]. The extent direction is defined towards the blade's tip. The damage is introduced in the FE model by a separation of nodes between elements at selected locations. The number of separated nodes and, with it, the length of the uncoupled element edges correspond to the damage extent. Figure 1 shows the location and the maximum disbond damage in the FE blade model. The influence of this damage on the dynamic behaviour can be assessed initially by numerical modal analysis. Relative differences between corresponding natural

frequencies of the healthy model and the damaged models give a first insight how responses may be affected. Furthermore, summing these differences for a chosen set of consecutive modes enables to estimate the change of the structural response signals for the frequency range between the related modes.

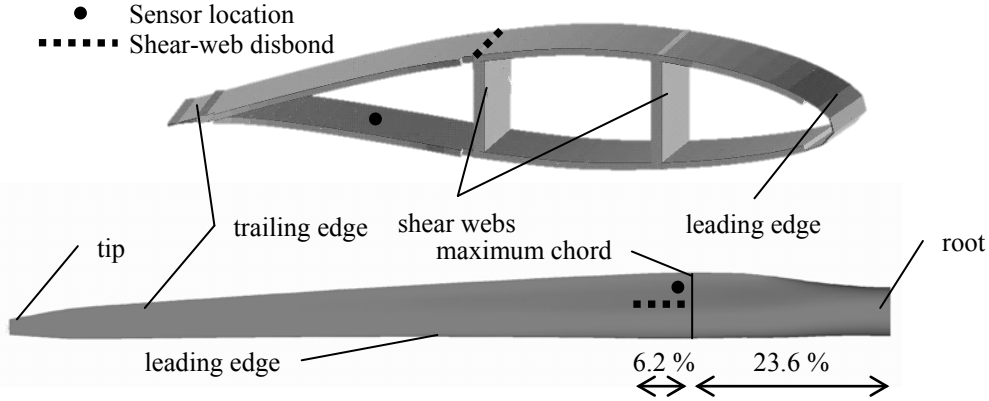


Figure 1: Location and maximum extent of shear-web disbond and location of ‘sensor’ for damage detection

The proposed damage detection method is based on time series analysis, thus transient simulations have been performed. The use of a realistic excitation is paramount for investigating the performance and applicability of the algorithm. The simulation is done for a parked WT situation, where only the motion of a single blade is considered and that of the tower is ignored. The generation of aerodynamic loads is done in three steps. Firstly, full-field wind data are generated with the NREL software TurbSim [20] according to IEC 61400-1 3rd Ed. [14]. The mean wind speed at hub height is chosen as the average wind speed of an IEC type I turbine with 10 m/s, and, for wind category B and the normal turbulence model, the turbulence intensity is 18.34 % for the inflow wind component. Secondly, aerodynamic loads are calculated with the NREL software AeroDyn and FAST [21, 22]. The blade element momentum theory is chosen to model the wake effect. Therefore, the blade is approximated by 17 strip elements, each of constant structural and aerodynamic properties. The results are time series of lift and drag forces,  $F_N$  and  $F_T$ , respectively, and pitching moments  $M_p$  at each element centre  $(x_r, y_r, z_r)$ . The application of these loads in the FE model is done in the third step. The mapping of element loads to nodal forces  $f_{x,i}$  and  $f_{y,i}$  of  $N$  surface nodes at positions  $(x_i, y_i, z_i)$  is based on [23], and it is illustrated in Figure 2. The equilibrium equations for forces and moments on a single blade element and related surface nodes are given with

$$\begin{aligned}
 F_N &= \sum_{i=1}^N f_{y,i} & M_p &= \sum_{i=1}^N (x_i - x_r) f_{y,i} & z_r F_N &= \sum_{i=1}^N z_i f_{y,i} \\
 F_T &= \sum_{i=1}^N f_{x,i} & 0 &= \sum_{i=1}^N (y_i - y_r) f_{x,i} & z_r F_T &= \sum_{i=1}^N z_i f_{x,i}
 \end{aligned}
 \tag{10}$$

The mapping is generally not unique. Therefore, it is chosen that only forces in y-direction produce non-zero pitching moments and the spatial distribution is assumed to be linear with

$$f_{x,i} = a_x (y_i - y_r) + b_x + c_x z_i, \quad f_{y,i} = a_y (x_i - x_r) + b_y + c_y z_i
 \tag{11}$$

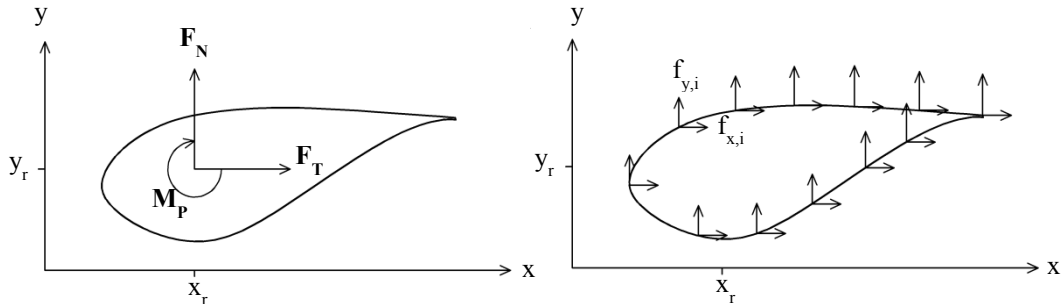


Figure 2: Element and nodal forces on a blade cross section

where  $a$  and  $b$  are the unknown coefficients describing the linear and constant distribution in the blade cross section, and  $c$  describes the linear distribution along the blade. The subscripts  $x$  and  $y$  denote the direction of the corresponding nodal forces. These coefficients can be obtained by solving the resulting linear system of equations. To reduce storage and computational efforts, coefficients of the load components have been calculated for each surface node in advance. During the transient simulation, only simple evaluations are necessary to obtain the nodal loads from the corresponding element forces for every time step. The simulation is done with a constant time step of 0.005 s.

**4 RESULTS**

The initial investigation of the dynamic behaviour is done by numerical modal analysis. The first three mode shapes and natural frequencies of the healthy blade are given in Table 1. The low natural frequencies correspond to a high flexibility of the blade.

Table 1: Numerical modal analysis results for the first three modes of the healthy blade.

Mode Description	Natural Frequency	Mode Shape of FE blade	
		Edge-wise View	Flap-wise View
1st flap-wise bending	0.869 Hz		
1st edge-wise bending	1.059 Hz		
2nd flap-wise bending	2.674 Hz		

Then, the effect of damage on natural frequencies of the FE blade model is investigated. The maximum extent of disbond for the numerical modal analysis is chosen to be approx. 3.82 m or 6.2% of the blade length, which corresponds to nine separated nodes. The effect on the  $i$ -th natural frequencies can be evaluated with the relative difference  $\Delta f_i$  between the frequencies of the healthy  $f_{b,i}$  and the damaged model  $f_{d,i}$  as

$$\Delta f_i = (f_{b,i} - f_{d,i}) / f_{b,i} \times 100\% \tag{12}$$

The results are shown in Figure 3, and it can be seen that the stacked sum of differences of the first ten modes and the damage extent has a nonlinear relationship. The highest contributions are from modes five and ten with the baseline frequencies 5.552 Hz and 12.716 Hz, respectively. Further, the sum of the stacked differences for damage extents less than approx. 3% is less than 1%, which shows early damage detection based on frequency shifts would be difficult.

Finally, transient simulations have been performed for the healthy model and for the nine damage extents of shear-web disbonding given above. The flap-wise and edge-wise accelerations at the nodes of the blade were obtained initially with durations of 630 s. However, for the damage detection, only the flap-wise accelerations of a selected node, measured by ‘sensor’ indicated in Figure 1, were used. The time series has been divided into 200 segments with 6000 samples and a shift of 600 samples. The segments have been standardized to reduce the variations due to the aerodynamic excitation using the segments estimated means and estimated standard deviations.

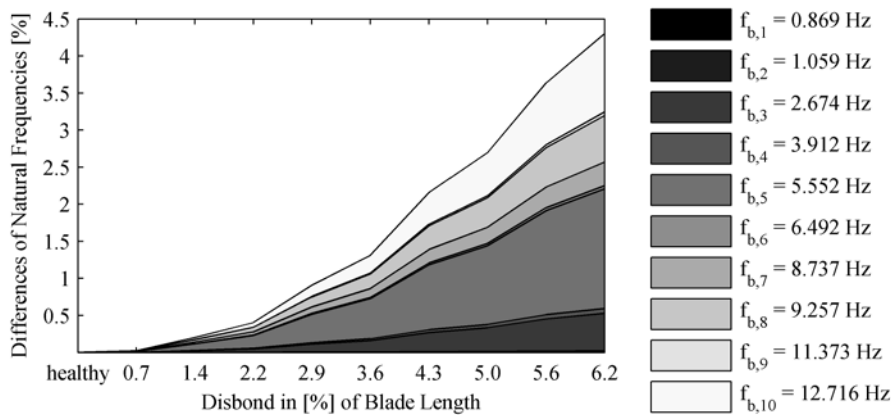


Figure 3: Stacked differences of natural frequencies with increasing damage

The influences of artificial noise and the number of coefficients on the DSF are assessed with the help of the Bayes error rate. The upper bound is calculated according to Eq. (2), where the healthy and the damaged classes had the same number of samples. Therefore, both probabilities,  $P_b$  and  $P_d$ , are set to 0.5.

Figure 4a shows the results for different artificial noise levels, which are introduced to the simulated signals as Gaussian random sequences with a standard deviation equal to the standard deviation of the initial signal multiplied by the noise-to-signal ratio. Artificial noise levels with noise-to-signal ratios between 2 % and 10 % were considered. The error rate is lower for signals contaminated with noise for the first damage extent. This is the case, because the noise leads to a higher deviation of the baseline model, thus the Mahalanobis distances increase even in the healthy state. For increasing disbond lengths, increasing noise levels result in higher error rates. Nevertheless, the error rates drop significantly for disbond length between 0.72% and 2.87% and become very small for higher damage extents. Thus, it is shown that the proposed DSF is only lightly affected by signal noise.

The results for different numbers of coefficients are shown in Figure 4b, where five coefficients are added for each row beginning with five. It can be seen that disbonding with more than 4% blade length can be detected with a misclassification rate below 10% in all cases with more than 5 coefficients. However, the number of autocorrelation coefficients is chosen to be 150 coefficients in order to achieve a low error rate for the hypothesis testing and to obtain a high sensitivity for small damages.

The hypothesis testing is done, as described above, with a baseline covariance matrix with 123 non-zero eigenvalues. The level of significance is chosen to be 5%, thus the distance limit for the healthy state is 149.88 for the cumulative distribution function  $F_{\chi^2_{23}}(1-0.05)$ . The results for the simulated damage extents are given in Table 2. In accordance to the Bayes error rate, the hypothesis testing demonstrates a clear identification of shear-web disbonding with lengths from 3.59% blade length for the given samples. Furthermore, the false alarm rate for the undamaged state is zero, but disbond damages with extents less than 2.87% cannot be detected safely.

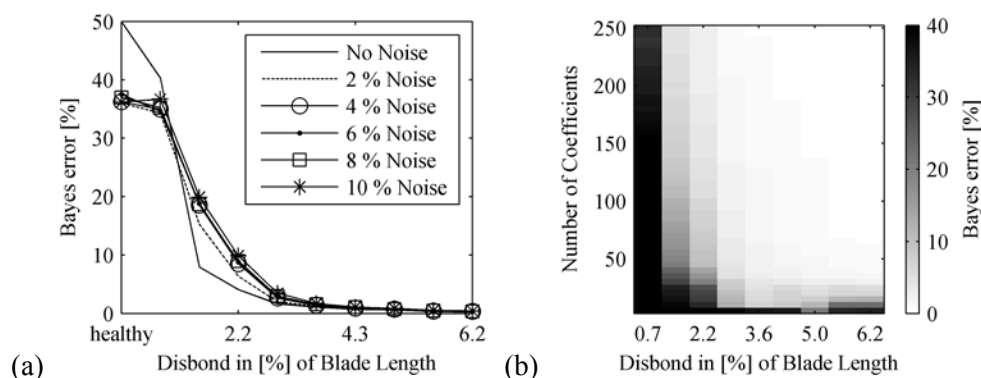


Figure 4: Effects on Bayes error rate; (a) Noise, (b) Number of Coefficients

Table 2: Results of hypothesis testing for the nine damage extents.

Damage extent in [%] of blade length		Absolute		Relative	
		Fail to reject $H_0$	Reject $H_0$	Fail to reject $H_0$	Reject $H_0$
0 %	$H_0$	200	0	1.0	0.0
0.72 %	$H_1$	200	0	1.0	0.0
1.44 %	$H_1$	198	2	0.99	0.01
2.15 %	$H_1$	165	35	0.825	0.175
2.87 %	$H_1$	5	195	0.025	0.975
3.59 %	$H_1$	0	200	0.0	1.0
4.31 %	$H_1$	0	200	0.0	1.0
5.03 %	$H_1$	0	200	0.0	1.0
5.62 %	$H_1$	0	200	0.0	1.0
6.20 %	$H_1$	0	200	0.0	1.0

## CONCLUSIONS

The present paper shows a damage detection method based on the Mahalanobis distance between vectors of autocorrelation coefficients calculated using acceleration signals. The method is applied to simulated data of a single FE WT blade with a shear-web disbonding damage scenario. The blade was excited with a simplified aerodynamic loading approach, where aerodynamic blade element loads were mapped to nodal forces of the FE model.

The DSF is assessed in two ways. Firstly, the upper bound of the Bayes error is used to investigate how noise and the number of coefficients affect classification results. The results showed that the effect of signal noise is dominating for small damages, and this is, therefore, important with respect to early damage detection. Furthermore, it is shown that high numbers of coefficients lead to lower error rates. Secondly, statistical hypothesis testing is done to obtain a decision about the structural state. The classification results are in accordance to the Bayes error rates. Additionally, damages from a certain disbond lengths could be detected with a high accuracy without false alarms for the healthy state.

The proposed DSF and the detection method have proven their potential for detection of shear-web disbonding. However, future work is required to increase the ability to detect small damages. Furthermore, in-operation simulations are necessary to improve the method for realistic conditions, and experimental validation is a prerequisite for the application in real WTs. Finally, for beneficial application in real WTs, damage localization and severity estimation are essential demands for future developments.



## ACKNOWLEDGEMENTS

Piotr Omenzetter and Simon Hoell's work within the Lloyd's Register Foundation Centre for Safety and Reliability Engineering at the University of Aberdeen is supported by Lloyd's Register Foundation. The Foundation helps to protect life and property by supporting engineering-related education, public engagement and the application of research.

## REFERENCES

- [1] The European Parliament and the Council of the European Union. The renewable energy directive 2009/28/EC. Official Journal of the European Union 2009; L 140.
- [2] Blanco MI. The economics of wind energy. *Renewable and Sustainable Energy Reviews* 2009; 13:1372-82.
- [3] Chou J, Chiu C, Huang I, Chi K. Failure analysis of wind turbine blade under critical wind loads. *Engineering Failure Analysis* 2013; 27:99-118.
- [4] Schubel PJ, Crossley RJ, Boateng EKG, Hutchinson JR. Review of structural health and cure monitoring techniques for large wind turbine blades. *Renewable Energy* 2013; 51:113-23.
- [5] Nair KK, Kiremidjian AS, Law KH. Time series-based damage detection and localization algorithm with application to the ASCE benchmark structure. *Journal of Sound and Vibration* 2006; 291:349-68.
- [6] Häckell MW, Rolfes R. Monitoring a 5 MW offshore wind energy converter - condition parameters and triangulation based extraction of modal parameters. *Mechanical Systems and Signal Processing* 2013; 40:322-43.
- [7] Ghoshal A, Sundaresan MJ, Schulz MJ, Pai PF. Structural health monitoring techniques for wind turbine blades. *Journal of Wind Engineering and Industrial Aerodynamics* 2000; 85:309-24.
- [8] Reynders E. System identification methods for (operational) modal analysis: review and comparison. *Archives of Computational Methods in Engineering* 2012; 19:51-124.
- [9] Fassois SD, Sakellariou JS. Time-series methods for fault detection and identification in vibrating structures. *Philosophical Transactions of the Royal Society A: Mathematical, Physical and Engineering Sciences* 2007; 365:411-48.
- [10] Bendat JS, Piersol AG. *Random data analysis and measurement procedures*, Hoboken, New Jersey: John Wiley & Sons, Inc., 2010.
- [11] Devijver PA, Kittler J. *Pattern recognition: a statistical approach*, Englewood Cliffs, NJ: Prentice Hall International, 1982.
- [12] Resor BR. Definition of a 5MW/61.5m wind turbine blade reference model 2013; SAND2013-2569.
- [13] Jonkman JM, Butterfield S, Musial W, Scott G. Definition of a 5-MW reference wind turbine for offshore system development 2009; NREL/TP-500-38060.
- [14] IEC Technical Committee 88: Wind turbines. International standard IEC 61400-3 2009.
- [15] Berg JC, Resor BR. Numerical manufacturing and design tool (NuMAD v2.0) for wind turbine blades: user's guide 2012; SAND2012-7028.
- [16] SAS IP Inc. ANSYS mechanical APDL. Release 14.5, 2012.
- [17] Jensen FM, Kling A, Sørensen JD. Scale-up of wind turbine blades - changes in failure type. *Proceedings of EWEA Annual Event (EWEA 2012)* 2012.
- [18] Jensen FM, Falzon BG, Ankersen J, Stang H. Structural testing and numerical simulation of a 34 m composite wind turbine blade. *Composite Structures* 2006; 76:52-61.
- [19] Ataya S, Ahmed MMZ. Forms of discontinuities in 100 KW and 300 KW wind turbine blades. *Proceedings of 10th World Wind Energy Conference & Renewable Energy Exhibition* 2011.
- [20] Kelley N, Jonkman B. TurbSim 2013. v1.06.00; last modified 30-May-2013; accessed 14-October-2013.
- [21] Laino DJ. AeroDyn 2013. v13.00.02a-bjj; last modified 23-February-2013; accessed 15-October-2013.
- [22] Jonkman J. FAST 2013. v7.02.00d-bjj; last modified 28-October-2013; accessed 28-October-2013.
- [23] Berg JC, Paquette JA, Resor BR. Mapping of 1D beam loads to the 3D wind blade for buckling analysis. *Collection of Technical Papers - AIAA/ASME/ASCE/AHS/ASC Structures, Structural Dynamics and Materials Conference* 2011.